Inactivation of the antidiabetic drug acarbose by human intestinal microbial-mediated degradation

Weihong Jiang (wjiang@cemps.ac.cn)

Key Laboratory of Synthetic Biology, CAS Center for Excellence in Molecular Plant Sciences, Shanghai Institute of Plant Physiology and Ecology, Chinese Academy of Sciences (CAS)

Research Article

Keywords: Gut microbiota, Acarbose, Klebsiella grimontii TD1, induced degradational inactivation

Posted Date: September 22nd, 2022

DOI: https://doi.org/10.21203/rs.3.rs-2086719/v1

Abstract

Gut microbiota plays an important role in drug modification, transformation and degradation, which are factors that need to be considered in personalized therapy. Acarbose, an inhibitor of α-glucosidase, is used as a first-line drug for the treatment of type 2 diabetes; however, its clinical effects vary greatly among individuals, and the underlying mechanisms relating to the contribution of gut microbes remain to be elucidated. Herein, we reported the association between acarbose resistance and enteric bacteria by analyzing clinical samples and anaerobic enrichment culture, and isolated a major acarbose-degrading gut strain, *Klebsiella grimontii* TD1. Metagenomic analysis of the intestinal microbiome found that the abundance of *K. grimontii* TD1 was higher in patients with weak acarbose response and increased with longer medication time. In addition, *in vivo* experiments using a diabetic mouse model showed that this strain significantly weakened the hypoglycemic effect of acarbose. Further, we identified a key acarbose-preferred glucosidase, Apg, in *K. grimontii*TD1 using a combined approach of induced transcriptome and protein profiling. This enzyme is structurally characteristic, could degrade acarbose into small molecules with loss of inhibitor function, and was widely distributed in intestinal microorganisms, especially in *Klebsiella*. These results indicate that the risk of acarbose resistance caused by metabolic degradation from intestinal bacteria is widespread in humans, and this "induced degradational inactivation" mechanism may be one of the main causes of non-antibiotic drug resistance.

Full Text

Type 2 diabetes mellitus (T2DM) is a common chronic metabolic disease, and its incidence is increasing globally year by year[1]. Acarbose is a first-line agent for the treatment of T2DM[2,3]; however, clinical data has shown obvious individual differences in the effect of the drug, with some patients developing severe drug resistance after long-term use[4,5], the mechanism of which is not fully understood. Acarbose has a pseudo-tetrasaccharide structure, which can compete with substrates to inhibit α-glucosidase, including α-amylase, sucrase, and maltosidase in human small intestinal epithelial cells, thereby reducing the metabolism of complex carbohydrates in food and postprandial blood glucose levels[6,7]. Concurrently, the majority of ingested acarbose cannot be absorbed through the human intestinal tract[8], thus potentially having a significant influence on the composition of gut microbiota[9-11].

There is often a bidirectional interaction between intestinal microbes and ingested drugs, including co-metabolism and modification[4,12-14]. Specific to acarbose, a group of newly discovered kinases in some bacterial members of the human oral and gut microbiome were found to selectively phosphorylate acarbose, resulting in its inactivation[4]. This work strongly supports a continued investigation of the influence of intestinal microbes on acarbose. Whether some specific gut microbes are enriched following long-term use of acarbose and in turn metabolize or utilize this drug, thus affecting its therapeutic efficacy merits further exploration.

In this study, we first identified key intestinal strains capable of degrading and inactivating acarbose through a stepwise anaerobic enrichment of clinical samples as well as analysis of data from an animal

model. Using a combination of bioinformatic, omics, and biochemical approaches, we further discovered and functionally characterized an unreported acarbose-preferred glucosidase that specifically degrades and inactivates acarbose in these intestinal strains, thereby revealing the potential causes and molecular mechanisms of such a non-antibiotic drug resistance phenomenon in clinical practice.

Results

Clinical analysis and discovery of the intestinal microbes for acarbose inactivation

A total of 499 patients recruited from five hospitals were screened for eligibility, and based on exclusion criteria, 393 patients of them were included in the primary analysis (Fig. 1). Clinical parameters (blood glucose and glycosylated hemoglobin levels) of these patients with T2DM treated with acarbose (Supplementary Data 1) were measured and analyzed to determine treatment efficacy. The findings showed significant individual differences in therapeutic efficacy (Fig. 2a). To determine the association between the efficacy of acarbose and gut microbiota, we randomly selected patients with high or low response to the drug (11 from each group), collected their intestinal microorganisms in fecal samples, and tested them in acarbose metabolism using a previously reported *ex vivo* system[15]. The results showed that the degree of acarbose degradation by the intestinal microbiota from the low-response group was significantly higher than that of the high-response group (Fig. 2b), suggesting that the difference in efficacy of acarbose may be caused by the metabolic capacity of intestinal microbiota.

Therefore, we attempted to search for the key intestinal strains associated with the degradation of acarbose. A fecal sample from the patient (within the abovementioned 22 patients) who showed the lowest drug response was collected and cultured anaerobically using a stepwise enrichment method (Fig. 2c). After five rounds of enrichment, the ability of intestinal microbiota to metabolize acarbose was significantly improved (Supplementary Fig. 1). Next, one aliquot of culture was plated on the solidified medium to isolate individual colonies, and then, a total of 76 isolates were picked out to test their ability in the degradation of acarbose. As expected, 18 isolates with high ability to metabolize acarbose were obtained, capable of degrading over 1.3 mg/mL acarbose within 24 h (Supplementary Fig. 2). Interestingly, a further identification using 16S rRNA gene sequencing and morphological analysis indicated that all these isolates belong to *Klebsiella grimontii*. We chose on isolate for genome sequencing (accession number: PRJNA801205) (Supplementary Fig. 3), and the result showed that it was distinct from the genome sequences of all reported *K. grimontii* strains. Thus, we termed it *K. grimontii* TD1. A following test revealed the efficiency of *K. grimontii* TD1 in acarbose metabolism, capable of degrading 0.5 mg/mL acarbose within 4 h (Fig. 2d). As a facultative anaerobe, *K. grimontii* mainly distributed in the small intestine, belongs to the phylum *Proteobacteria*, and accounts for more than 1% of total intestinal microbiota[16]. Coincidentally, acarbose mainly targets multiple amylases and glucosidases in small intestinal epithelial cells[15], which is spatially beneficial to its interaction to *K. grimontii* TD1 as well as metabolic degradation by this strain.

Correlation between the abundance of K. grimontii TD1 in intestinal microbiota and the efficacy of acarbose

To determine the abundance of *K. grimontii* TD1 in the human intestinal tract and its causal relationship with the therapeutic efficacy of acarbose, fecal samples were collected from the abovementioned 393 clinical acarbose-treated patients that were divided into high and low response groups according to their blood glucose levels for metagenomic sequencing analysis. The results showed that the average abundance of *K. grimontii* TD1 in the high-response group was significantly lower than in the low-response group (Fig. 2e), indicating that the quantity of this strain in the human gut microbiota was negatively correlated with drug efficacy, which may be attributed to its ability to degrade acarbose.

Subsequently, we further analyzed the dynamic changes of intestinal microbial metagenome in patients who underwent different acarbose-treated periods. The results showed that the patients who took the agent for less than 12 months had the lowest abundance of *K. grimontii* in their intestines (Fig. 2f); as the duration of administration of acarbose prolonged, the relative abundance of *K. grimontii* TD1 in patients' intestines gradually increased over a period of 12 months to 36 months (Fig. 2f). These findings indicate a dynamic induction and enrichment effect of acarbose on this strain.

Influence of K. grimontii TD1 on the effects of acarbose in a T2DM mouse model

The aforementioned *in vitro* studies showed that *K. grimontii* TD1 effectively degraded acarbose and was thus potentially associated with a reduced therapeutic effect. Therefore, we further investigated the impact of this strain on the efficacy of acarbose in treating animals with T2DM. First, we constructed a High Fat Diet/Streptozotocin (HFD/STZ)-induced T2DM mouse model by administering a high-fat diet and a streptozotocin (STZ, 40 mg/kg body weight) injection to C57BL/6J mice (Fig. 2g). The body weights of the high fat diet-induced mice increased significantly compared with the normal diet control animals, but after the streptozotocin injection, all the mice experienced a body weight reduction in a short period (Fig. 2g). Mice with fasting blood glucose (FBG) levels > 14 mM were screened as having T2DM and divided into four groups for either acarbose or *K. grimontii* TD1 administration by gavage every day for two weeks. Next, the mice were fasted overnight and administered PBS, acarbose, *K. grimontii*, and *K. grimontii* + acarbose as well as a starch solution (1.0 g/kg) by gavage. The cumulative serum glucose levels were determined over a period of 240 min (0, 60, 120, 180, and 240 min) to evaluate the anti-diabetic effect of acarbose. As depicted in Fig. 2h, the cumulative serum glucose level in mice with T2DM were significantly reduced following gavage of acarbose at 60 and 120 min after starch loading. However, this suppressive effect from acarbose on postprandial hyperglycemia was decreased in mice administered *K. grimontii* TD1 and acarbose. Simultaneously, the areas under the glucose response curve (AUC) of acarbose treatment groups were also affected by the addition of *K. grimontii* TD1, becoming comparable to effects of *K. grimontii* TD1 alone (Fig. 2i). Overall, these results demonstrated that *K. grimontii* TD1 degraded acarbose and reduced its anti-diabetic effect.

Discovery, characterization, and analysis of acarbose-preferred glucosidase (Apg)

Both animal experiments and metagenomic analysis of intestinal microbes from patients supported that *K. grimontii* is the main species involved in degrading acarbose. Therefore, we sought to elucidate the key enzyme(s) responsible for this metabolic process. To this end, two different strategies were adopted.

Firstly, we designed an acarbose-induced transcriptional profile to rapidly find potentially essential genes for acarbose inactivation. In brief, *K. grimontii* TD1 was cultured in the M9 medium using starch instead of glucose as the sole carbon source. When acarbose was added into the medium, the amylase activity in *K. grimontii* TD1 was inhibited, and thus, the strain could not effectively metabolize starch to support its growth. To survive, *K. grimontii* TD1 would enhance the expression of the enzymes capable of inactivating acarbose, aiming to resume starch utilization (Fig. 3a). Based on this principle, a comparative transcriptomic analysis based on RNA-seq was carried out and we observed that after adding 2 mg/mL of acarbose to the medium, 36 genes exhibited over 20-fold upregulation in *K. grimontii* TD1 (Fig. 3b, Supplementary Fig. 4, Supplementary Table 1), indicating that these genes may be associated with acarbose metabolism.

Furthermore, a combination of multiple protein separation techniques was used to search for target enzymes. We observed that, when the lysed total protein of *K. grimontii* TD1 was incubated with acarbose for several hours, the concentration of acarbose in the mixture was significantly reduced (Fig. 3c), indicating that the acarbose-degrading protein(s) of interest was present. Next, three rounds of preliminary separation were carried out by several Fast Protein Liquid Chromatography (FPLC) techniques (ion-exchange and molecular sieve) (Supplementary Fig. 5); and the obtained components with high acarbose-degrading activity were further separated using SDS-PAGE followed by a tracking determination of enzyme activity (Supplementary Fig. 6). Encouragingly, we observed a specific protein band of ~ 70 kDa in both the fraction 28 and 29 that showed higher acarbose-degrading activities (Supplementary Fig. 6). Following this, the corresponding gel bands were cut out and subjected to proteomic analysis. A total of 108 candidate proteins were obtained (Supplementary Table 2), among which 58 showed higher abundance (more than one million) (Supplementary Table 3). The genes coding for these 58 proteins were further compared to the abovementioned 36 genes with ≥ 20-fold upregulation in the presence of acarbose in the comparative transcriptomic analysis. Promisingly, only one protein annotated as maltodextrin glucosidase (encoded by the L5654_016645 gene) was found in both cases (Fig. 3d). This gene was then cloned and expressed in *E. coli* BL21 (de3), and as expected, the resulting recombinant strain was able to metabolize acarbose (Supplementary Fig. 7). Simultaneously, the expressed protein product of this gene was purified for enzyme activity assay, and its activity towards acarbose degradation was also observed (Fig. 3e). Consequently, an acarbose-preferred glucosidase was discovered from intestinal bacteria and it was named Apg.

Interestingly, we found that acarbose could be degraded by Apg into two products. The chemical structures of these two compounds were further identified as acarviosine-glucose and acarviosine

(Supplementary Fig. 8). These findings suggest that Apg is a novel glycosidase capable of hydrolyzing both acarbose and acarviosine-glucose, yielding acarviosine-glucose and acarviosine in a theoretical ratio of 1: 2, respectively (Fig. 3f; Supplementary Fig. 8a). To clarify whether Apg-catalyzed acarbose degradation is associated with the disruption of acarbose efficiency, we investigated the influence of acarviosine-glucose and acarviosine on porcine pancreatic amylase. As depicted in Fig. 3g, compared to acarbose, acarviosine-glucose exhibited approximately 20% reduced inhibition on the activity of α-amylase, while acarviosine almost completely lost inhibition ability. Therefore, all these results revealed the mechanism by which Apg deactivates the effect of acarbose through a two-step hydrolysis process. This is an unreported acarbose-degrading pathway in intestinal bacteria.

We also analyzed the optimum reaction conditions and kinetic constants of Apg. The results showed that the optimum pH and temperature of this enzyme under anaerobic conditions were 7.5 and 37°C, respectively (Supplementary Fig. 9a, b), which are similar to the human intestinal environment. The k_{cat}/K_m value of Apg was 2.197×10^6 $M^{-1}\cdot s^{-1}$ (Fig. 3h), indicating that Apg had a strong ability to catalyze the degradation of acarbose. To understand the preference of Apg in relation to different substrates, we selected six substrates for testing, including maltopentaose, maltotetraose, maltotriose, starch, maltose, and isomaltotriose. The results showed that Apg could catalyze the degradation of short-chain oligosaccharides such as maltopentaose, maltotetraose, and maltotriose, but could not act on long-chain starches and short-chain disaccharides (Fig. 3i).

Structural and functional characteristics of Apg

To explore the molecular basis of the Apg-catalyzed hydrolysis of acarbose, the 3D structure of Apg was modeled using the crystal structures of its homologous proteins (Fig. 4a and Supplementary Table 4). Its catalytic residues were assumed to be D336 (the nucleophile), E373 (the proton donor), and D448 (the transition state stabilizer)[18]. The homology modeling result suggested that the arrangement of residues in the catalytic site of Apg is different from that of human α-amylase. In Apg, the distance between the catalytic residues and the margin of the pocket (defined by H209) is 9.5 Å, whereas the nucleophile D197 of human α-amylase is as close as 5.3 Å to the margin of the pocket defined by Y62 (Fig. 4b) according to the crystal structure (PDB ID: 1XCX). Furthermore, molecular docking simulation suggested that the former can accommodate two sugar rings, orienting the nucleophile D336 towards the C1 of the second ring of the non-reducing end of acarbose (first column of Fig. 4c, ΔG = − 12.07). Acarbose forms multiple hydrogen bonds with the catalytic residues and other residues nearby (e.g., H209, R496, and Y393), which would facilitate the reaction to yield the two-ring product acarviosine. Meanwhile, there is another binding mode of the Apg-acarbose complex (Fig. 4c, second column; ΔG = − 11.74), where the first ring moves to the open space beyond H209 and poses the catalytic spot at the linkage between the third and the fourth rings, yielding the three-ring product acarviosine-glucose. Plugged into the equation of binding free energy (ΔG) and the equilibrium constant, the ratio of the two-ring product over the three-ring product was estimated to be 1.75:1, which was in concordance with the experimental ratio of 2:1. In contrast, the co-crystal structure of acarbose and human α-amylase complex (Fig. 4d) revealed a different binding mode. Because of the limited space which only accommodates the first ring of acarbose (Fig. 4b, bottom), the

uncleavable linkage between the first two rings is posed beside the nucleophile D197 (Fig. 4e). All these results suggest a different position of the catalytic residues within the ligand-binding pocket of Apg from that of human α-amylase, which enables its hydrolytic cleavages at the α-(1,4) linkages of acarbose.

By leveraging the molecular docking technique, we elucidated the inhibition potential of acarbose and its degradation products (i.e., acarviosine-glucose and acarviosine) against human α-amylase. The docking results reproduced the binding mode of acarbose from the crystal structure, showing broad hydrogen bonding with D197, D300, E233, K200, E240, and G238 (Fig. 4e, left). The ΔG was predicted as − 10.25 kcal/mol. Compared with acarbose, acarviosine-glucose adopted the same binding pattern and orientation, with the exception of one less hydrogen bond with G238 at the edge of the pocket, resulting in a slightly higher ΔG of − 9.08 kcal/mol (Fig. 4e, middle). However, the inactive product, acarviosine, could only occupy half of the entire pocket and formed much weaker polar interactions, resulting in an unfavorable ΔG of − 6.32 kcal/mol (Fig. 4e, right), which explained its poor inhibition against α-amylase. Altogether, through molecular modeling approaches, we observed a different arrangement of residues in the active site of Apg compared with human α-amylase, showing a favorable hydrolytic site between the second and third rings of acarbose. Moreover, the product was inactive due to a lack of occupation of the α-amylase pocket.

Distribution and abundance of Apg in intestinal microbiota

We investigated the distribution of Apg-like enzymes in microbial communities using the Apg sequence as the query. The BLASTp search identified 1,415 putative Apg-like enzymes (amino acid identity ≥ 80%, coverage ≥ 80%, e-value ≤ 1e − 10) from 456 microbial species (Supplementary Data 2). Next, a maximum likelihood phylogenetic tree of Apg homologues was constructed (Fig. 4f; Supplementary Fig. 10), showing that the Apg-like enzymes exist across at least ten genera. Among them, *Klebsiella* occupied the largest proportion.

To further characterize the distribution of the *apg* genes in the human intestinal microbiota, we analyzed 393 abovementioned metagenome samples and 5,372 healthy human intestinal bacterial metagenome samples (from GMrepo)[19] of individuals from different countries and of different genders and weights. The results showed that *apg*$^+$ bacteria were observed in 14.2% and 98.4% of the healthy and acarbose-treated T2DM samples, respectively (Fig. 4g), indicating that *apg*$^+$ bacteria are widespread in intestinal microbiota. Furthermore, the abundance of *apg* in acarbose-treated samples (ranging from 0 to 7% with an average abundance of 0.8%) was significantly higher than that in healthy samples (ranging from 0 to 0.7% with an average abundance of 0.02%) (Fig. 4g, Supplementary Fig. 11), suggesting that *K. grimontii* was enriched by acarbose treatment. However, the abundance of *apg* varied greatly among different populations, which may be due to the differences in host physiological status or geographical environment. This was also one of the important factors for observed individual differences in acarbose-treated patients. For example, the prevalence of Apg$^+$ bacteria in female gut microbiota was slightly higher than that in male (Supplementary Fig. 12a), but the distributions of their abundance are similar (Supplementary Fig. 12b). Among different ethnic groups, Apg$^+$ bacteria are most popular in Chinese,

with a prevalence of 48%, whereas only 3.6% and 3.7% are shown in Canadian and Danish samples, respectively (Supplementary Fig. 12c). The German samples have the highest median abundance (Supplementary Fig. 12d). In addition, the obese population with a body mass index (BMI) of over 30 contains significantly less Apg^+ samples (2.2%) compared with the normal group (BMI: 18.5 ~ 24.9, Apg prevalence: 9.5%) (Supplementary Fig. 12e), although their distributions of abundance are similar (Supplementary Fig. 12f). However, there was no correlation between Apg prevalence and age (Supplementary Fig. 12g, h). Overall, our findings show that Apg-like enzymes are a widely distributed and differentially prevalent class of hydrolases in the gut with a pervasive effect on the metabolism of acarbose and short-chain oligosaccharides.

Discussion

Our study revealed a novel mechanism of “induced degradational inactivation” of acarbose, which is a representative case of non-antibiotic drug resistance mediated by intestinal microorganisms. Notably, microbes responsible for acarbose catabolism are found to be widespread in the human intestinal tract, which on the one hand reflects the functional diversity of the gut microbiota, but also implies hidden danger of drug resistance, especially with the prolongation of medication time.

Generally, glucosidases can be inhibited by the drug acarbose in diabetic patients to achieve hypoglycemic effect, but we found that intestinal microbes encode a kind of unreported “acarbose-preferred glucosidases”, Apg, that can significantly degrade acarbose into acarviosine-glucose and acarviosine, thereby disrupting acarbose efficiency. In this case, the role of acarbose altered from being an inhibitor to an available substrate. This interesting “break defense” phenomenon may be required by gut bacteria to protect them against the adverse effects of acarbose. For example, it has been reported that acarbose inhibits the utilization of starch by *Bacteroides thetaiotaomicron* and *Bacteroides fragilis*, thus affecting the composition of gut microbiota[18]. In addition, acarbose has been found to regulate bile acid metabolism by modulating gut probiotic abundance[7]. A recent study by Donia’s group observed that microbes of the human oral cavity and gut encode enzymes which can phosphorylate and inactivate acarbose[13]. Specific to *K. grimontii* TD1, its role in the degradation of acarbose has been demonstrated by our *in vitro* culturing and *in vivo* animal experiments, confirming that its accumulation can be induced by acarbose. Besides, this strain was found to mainly colonize small intestine, which is just the main region where acarbose plays its anti-α-glucosidase role[17]. Therefore, it can be speculated that the acarbose-degrading bacteria in the intestinal tract may obtain growth advantages and continuous enrichment while eliminating acarbose interference. Of course, it’s unlikely that *K. grimontii* TD1 is the only member of the gut microbiota which can degrade acarbose. Our work strongly supports a continued investigation of acarbose-degrading gut bacteria as well as related metabolic mechanisms, thereby achieving a more comprehensive understanding of microbiome-acarbose interaction.

Furthermore, structural simulation analysis showed that Apg, as a special glucosidase, preferentially degraded acarbose rather than other starchy substrates, because the positions of its catalytic residues in

the ligand binding pocket were different from those of human α-amylase, making it more suitable to bind to and interact with acarbose. Such a unique protein structure not only helps to understand the distinct catalytic mechanism of this enzyme, but also provides a potential target for the design of inhibitors that can block this enzyme *in vivo*.

In summary, this work identified an unreported glucosidase-initiated acarbose-degrading pathway in intestinal bacteria. Our finding, in combination with Donia's report regarding kinase-mediated acarbose inactivation[4], strongly suggests that the interaction between acarbose and intestinal microbiota is diverse[7], and moreover, there may be more mechanisms contributing to acarbose resistance. Under certain conditions, gut microbiota may use one of the main mechanisms, or several ways of coexistence to support their survival, which needs more clinical case analysis and in-depth research to elucidate the underlying mechanisms, thus guiding precision medicine.

Materials And Methods

Eligibility criteria for selecting studies and pretreatment of fecal samples

Patients with T2DM, defined according to the 1999 WHO criteria based on oral glucose tolerance test, were recruited from five hospitals in Henan province (Fig. 1 and Supplementary Data 1). All patients were treated with acarbose and have voluntarily signed informed consent before enrollment. Those with one or more of the following characteristics were excluded: severe gastrointestinal disease; history of intestinal surgery or abdominal surgery; participants who had been treated within the last three months with immunosuppressive agents, steroids, antidiarrhea agents, antibiotics, and/or other gastrointestinal motility agents; severe liver dysfunction (serum alanine aminotransferase concentration more than 2.5 times above upper limit of normal range); abnormal renal function (eGFR < 60 ml/min/1.73m^2); history or presence of cancer; other severe conditions which would put the patients in high risk during the study. A total of 499 patients were screened for eligibility, in which 393 patients (57.5% male, mean age 57.1) were included in the primary analysis based on exclusion criteria. A flowchart for the inclusion of the participants is shown in Fig. 1. The samples were obtained with informed consent from all participants or their legal guardians. The study was approved by the Ethics Committee of the First Affiliated Hospital of Zhengzhou University (2021-KY-1180-002).

General characteristics of the patients with T2DM who received acarbose treatment are listed in Supplementary Data 1. Groups are mainly based on the levels of blood glucose and HbA1c after acarbose treatment. Patients with acarbose treatment-sensitive (high-response, N = 93) and non-sensitive (low-response, N = 217) were subjected to the analysis of their stool samples. All participants with diabetes have signed an informed consent form. Freshly collected human fecal material from the volunteers (< 10 min from collection, transported on ice) was immediately brought into an anaerobic chamber (75% N_2, 10% CO_2, 15%H_2) (Thermo Forma, Inc., Waltham, MA, USA). Three grams of the sample

were suspended in 25 mL of sterile phosphate buffer (8 g/L of NaCl, 0.2 g/L of KCl, 1.44 g/L of Na_2HPO_4, and 0.24 g/L of KH_2HPO_4) supplemented with 0.1% l-cysteine (PBSc) in a 50 mL sterile tube. The mixture was left standing still for 5 min to let insoluble particles settle. The supernatant was further mixed with an equal volume of 40% glycerol in PBSc. Aliquots (1 mL) of this suspension were placed in sterile cryogenic vials and frozen at − 80 ℃ for the following experiments[15].

Evaluation of acarbose degradation by the fecal microbiome from diabetics

The ex vivo culturing of the gut microbiome from patient samples was carried out as described previously[15]. All the manipulations were carried out in an anaerobic chamber (Thermo Forma, Inc., Waltham, MA, USA). Briefly, 200 µL of each glycerol stock from the abovementioned fecal samples was inoculated into 5 mL of modified GAM Broth Medium (mGAM) for inoculum preparation. After 12 h of cultivation at 37 ℃, 200 µL of inoculum was transferred into 5 mL of mGAM medium supplemented with acarbose (1.8 mg/mL). The culture was incubated at 37 ℃ for 24 h and then centrifuged at 14,000 *g* for 10 min at 4 ℃. The obtained supernatant was used for HPLC analysis to determine the residual acarbose amount.

HPLC analysis of acarbose and other sugars

The concentration of acarbose was determined using high-performance liquid chromatography (HPLC) (Agilent 1260 infinity HPLC system) with a ZORBAX SB-C18 column (particle size, 5 µm; 250 mm × 4.6 mm) (Agilent Technologies, Santa Clara, USA) and a UV diode array detector (Agilent Technologies, Santa Clara, USA). The analysis was carried out under the following conditions: the column temperature was maintained at 50 ℃. Solution A (H_2O) and solution B (methanol) served as the mobile phases to form a gradient as follows: 3–50% solution B for 0–25 min, 50–3% solution B for 25–25.1 min, and 3% solution B for 25.1–30 min. The flow rate was 1 mL/min. The injection volume was 10 µl. The UV detection wave length was 210 nm. The concentrations of samples were calculated according to peak area-based calibration curves of various concentrations of acarbose standards.

The concentrations of glucose, xylose, and fructose were determined using a high-performance liquid chromatography (HPLC) (Agilent 1100 series) equipped with a Bio-Rad Aminex HPx-87H column (1, 300 mm × 7.8 mm) and a refractive index detector. The analysis was carried out with 5 mM H_2SO_4 as the mobile phase at a rate of 0.6 mL/min. The column temperature was set to 35 ℃.

Enrichment cultivation and isolation of acarbose-degrading strains

A fecal sample from an acarbose-resistant patient was pretreated as described above. All the manipulations were carried out in an anaerobic chamber (Thermo Forma, Inc., Waltham, MA, USA). Briefly, 200 µL of glycerol stock from the abovementioned fecal samples was transferred into mGAM medium

containing 0.01 mg/mL acarbose. The culture was incubated at 37 ℃ for 12 h and then passaged twice by a 1: 20 dilution into fresh mGAM medium containing 0.01 mg/mL acarbose. Each successive passage was incubated for 24 hours. Next, the culture was transferred into mGAM medium containing 0.1, 1, 10, and 20 mg/mL acarbose in the proper order and handled following the same steps as above described. These final enrichment cultures were diluted to different concentrations and streaked onto mGAM agar plates. After 24 h of incubation at 37 ℃, a certain number of colonies appeared on agar plates and were then picked separately and inoculated into the liquid mGAM medium containing 10 mg/mL acarbose. After 24 h of incubation at 37 ℃, the cultures were centrifuged at 14,000 *g* for 10 min at 4 ℃. The obtained supernatanta were used for HPLC analysis to determine acarbose concentrations.

Once acarbose in the medium was found to be consumed, the corresponding colonies that displayed activity were picked out for sequencing (accession number: PRJNA801205). Here, we identified *Klebsiella grimontii* TD1 as an active acarbose-degrading strain in the human gut microbiome. This strain was inoculated into liquid mGAM medium (containing 1.5 mg/mL of acarbose) to ensure its acarbose degradation ability. Simultaneously, the grown *K. grimontii* TD1 cells were harvested by centrifugation at 4,000 *g* for 10 min at 4 ℃ and then stored at −20 ℃ for the following experiments.

Animal studies

Four-week-old male C57BL/6J mice were purchased from Charles River Laboratories China (Beijing, China). The animals were maintained under controlled temperature, humidity, and lighting conditions (12-hour light: 12-hour darkness cycle) with free access to food and water. All experiments were performed according to the ethical guidelines of the Institute of Neuroscience, Chinese Academy of Sciences (ethical review approval number: NA-041-2021-R1). The establishment of high-fat diet (HFD)/Streptozotocin (STZ)-induced T2DM mice was performed based on the previous method[21]. After one-week acclimatization period, the mice were randomly divided into two groups: (i) NC (n = 9), the normal control fed a standard chow diet; (ii) HFD (n = 60), the high-fat diet control fed a diet with 60 kcal% Fat (Research diet, New Brunswick, NJ, USA; D12492). After 12 weeks of treatment, the mice of the HFD group were fasted overnight and intraperitoneally injected with a single dose (40 mg/kg body weight) of freshly prepared STZ (Cayman Chemical Co., USA) solution for five consecutive days. After two weeks, the fasting blood glucose (FBG) was assayed by tail vein blood sampling using a blood glucose Accu-Chek Performa (Roche Diagnostics). The mice with FBG > 14 mM were selected as T2DM and divided into four groups: PBS, acarbose, *K. grimontii* TD1, and *K. grimontii* TD1 + acarbose groups. The PBS group (T2DM + PBS, n = 11) was gavaged with PBS solutions; the acarbose group (T2DM + acarbose, n = 11) was treated with 50 mg/kg/day acarbose (Sinopharm Chemical Reagent Beijing Co. Ltd) by gavage; the *K. grimontii* TD1 group (T2DM + *K. grimontii* TD1, n = 10) was gavaged with 1×10^{11} CFU viable cell of *K. grimontii* TD1; the acarbose + *K. grimontii* TD1 group (T2DM + acarbose + *K. grimontii* TD1, n = 10) was gavaged with 50 mg/kg/day acarbose as well as 1×10^{11} CFU *K. grimontii* TD1. All the mice were gavaged once per day for two weeks. On the fourteenth day, all the mice in the four groups were fasted overnight and gavaged as abovementioned in the next morning. Additionally, a starch solution (1 g/kg) was gavaged to all the mice at the same time. The tail vein blood glucose at 0, 60, 120, 180, and 240-min post-

gavage was assayed with the blood glucose Accu-Chek Performa (Roche Diagnostics). Then, the incremental glucose levels at different time points were calculated. The areas under the glucose response curve (AUCs) were calculated using GraphPad Software (GraphPad Prism version 7.0).

RNA-Seq and data analysis

The *K. grimontii* TD1 strain was grown in MS medium (34.0 g/L Na_2HPO_4, 15.0 g/L KH_2PO_4, 2.5 g/L NaCl, 5.0 g/L NH_4Cl, 2 ml 1M $MgSO_4$, 20 ml 20% starch, 0.1 ml 1M $CaCl_2$) with (2 mg/mL) or without the supplementation of acarbose. The cells at the logarithmic phase of growth were harvested by the centrifugation at 4,000 *g* for 10 min at 4 ℃ and then frozen immediately in liquid nitrogen.

Total RNA was extracted using the TRIzol® Reagent kit (R0016, Beyotime, Shanghai) according to the manufacturer's protocol and the residual DNA was eliminated using DNase I (Takara). RNA concentration was determined using a NanoDrop spectrophotometer (Thermo Fisher Scientific, Waltham, MA). High-quality RNA samples were used to construct sequencing libraries.

RNA-seq transcriptome library was established using the TruSeq™ RNA sample preparation Kit from Illumina (San Diego, CA) according to the manufacturer's instructions using 2 μg of total RNA. Briefly, ribosomal RNA (rRNA) depletion instead of poly adenylation selection is adopted to enrich RNA suing a Ribo-Zero Magnetic kit (epicenter). The obtained mRNAs were broken into short fragments (200 nt). Then, cDNA was synthesized via reverse transcriptase using a SuperScript double-stranded cDNA synthesis kit (Invitrogen, CA) with random hexamer primers (Illumina). The second strand of cDNA was generated by incorporating deoxyuridine triphosphate (dUTP) in place of deoxythymidine triphosphate (dTTP), aiming to create blunt-ended cDNA. The yielding double-stranded cDNA was subjected to end-repair, phosphorylation, and 3' adenylation and adapter ligation in sequential. The second strand of cDNA with dUTP was degraded using UNG enzyme (Uracil-N-Glycosylase). The cDNA fragments of 200 bp on 2% Low Range Ultra Agarose were purified and then used for PCR amplification using Phusion DNA polymerase (NEB) for 15 reaction cycles. After quantified using a micro fluorometer (TBS-380, TurnerBioSystems, USA), the library was sequenced on the Illumina HiSeq × Ten sequencer using paired-end sequencing. Processing of original images for sequences base-calling and calculation of quality value were performed using the Illumina data processing pipeline (version 1.6), thereby generating 150-bp paired-end reads. A Perl program was written to filter low-quality sequences and reads with more than 5% of N bases (unknown bases) or containing adaptor sequences.

The generated raw data were used for bioinformatics analysis. All the analyses were performed using the free online platform of Majorbio Cloud Platform (www.majorbio.com) from Shanghai Majorbio Bio-pharm Technology Co., Ltd. The software and parameters are the same as previously described[22].

qRT-PCR was conducted to verify RNA-Seq data,. Briefly, grown cells after 24 h cultivation were harvested, frozen quickly in liquid nitrogen, and then ground into powder. RNA samples were extracted with the Ultrapure RNA Kit (SparkJade, Shanghai, China), followed by digestion with DNase I (SparkJade, Shanghai, China) to remove residual chromosomal DNA. qRT-PCR was carried out in a MyiQ2 thermal

cycler (Bio-Rad, USA) using a SYBR Green PCR premix kit (SparkJade, Shanghai, China). The relative transcript levels of target genes were normalized to *gapA* (*L5654_11535*, an internal control), and the relative fold changes in transcription (tested strains versus control strains) were determined as previously described[23]. The experiments were conducted with three independent RNA samples (biological replicates). The primers used are listed in Supplementary Table 5.

Fast protein liquid chromatography (FPLC) and liquid chromatography–tandem mass spectrometry (LC-MS/MS) analyses

FPLC was used to purify target enzymes. First, 250 μL of the frozen stock of *K. grimontii* TD1 was inoculated into 300 mL of liquid mGAM medium and grown at 37 ℃ for 12 h. The grown cells were harvested by centrifugation at 4,000 *g* for 5 min at 4 ℃ and resuspended in 10 mL of buffer (50 mM Tris-HCl, 100 mM NaCl, 10% glycerol, pH 7.9). Resuspended cells were lysed through a cell disruptor (French Press, Constant Systems Limited, UK). The lysates were then clarified by centrifugation (14,000 *g* for 1 h at 4 ℃) and the supernatant (400 μL) was subjected to protein purification using FPLC (AKTA PURE,GE healthcare, UK) with an anion column (Hitrap™ Q HP, GE healthcare, UK). Solution A (50 mM Tris-HCl, 50 mM NaCl, 1% glycerol, pH 7.9) and solution B (50 mM Tris-HCl, 1 M NaCl, 1% glycerol, pH 7.9) were used as the mobile phases to form a gradient as follows: 0–100% solution B for 0–30 min at a flow rate of 3 mL/min. Samples were collected every two minutes for the measurement of acarbose-degrading activity.

The fractions (Q16-Q18) with acarbose-degrading activities were subjected to FPLC for another round of purification using a cation column (Hitrap™ SP HP, GE healthcare, UK) via the same procedure as above described, yielding further subdivided active fractions (H27-H31).

Finally, the fractions H27-H31 were concentrated 5-fold using a spin concentrator with a 10 kDa cutoff (4, 000 *g* for 1 h at 4 ℃) and then subjected to FPLC for size-exclusion chromatography using a molecular-sieve column (Hiload 16/600 Superdex 200, GE healthcare, UK). The fraction was eluted using a mobile phase (pH 8.0, 50 mM Tris-HCl, 100 mM NaCl, and 1% glycerol) and a flow rate of 0.3 mL/min. Samples were collected every 0.5 mL outflow and subjected to the measurement of acarbose-degrading activity. Next, all the samples were run on SDS-PAGE, and the gel bands that only occurred in the samples with acarbose-degrading activity were cut out and purified for LC-MS/MS analysis, aiming to confirm protein identities within the bands and assess the presence of the target enzymes for acarbose degradation (Supplementary Table 6). The analyses were carried out by Applied Protein Technology (Shanghai, China) on a high pH reverse-phase high-pressure liquid chromatography (HPLC) (Thermo Scientific, Vilnius, Lithuania) followed by a Q Exactive mass spectrometer (Thermo Scientific, Vilnius, Lithuania) as previously described[24]. The UniProt database of *Klebsiella grimontii* (https://www.ncbi.nlm.nih.gov/bioproject/PRJNA605147) was searched using Mascot (v.2.3.02, Matrix Science).

Construction of plasmids

All the primers, plasmids, and strains used in this study are listed in Supplementary Tables 5 and 6, respectively.

The vector expressing the gene (L5654_01665) encoding the acarbose hydrolase from *K. grimontii* TD1 in *E. coli* DH5α was constructed as follows. The DNA fragment of the gene was obtained by PCR amplification using the *K. grimontii* genomic DNA as the template and the primers L5654_01665-f/ L5654_01665-r. The PCR product was analyzed by agarose gel electrophoresis and the target band was recovered using a DNA gel recovery kit (Axygen Biotechnology Company Limited, Hangzhou, China). The yielding DNA fragment was linked with the linear plasmid pET28a vector (digested with NdeI and XhoI) using a Hieff Clone Plus One Cloning Kit (10912ES10, Yeasen, China), generating the target plasmid pET28a- L5654_01665. The constructed plasmid was checked by DNA sequencing.

The plasmids expressing the other genes (Supplementary Table 6) from *K. grimontii* TD1 were constructed with the same steps except for the primers used in PCR amplification.

Protein production and purification

The plasmids harboring the coding sequences of the target proteins were transformed into *E. coli* BL21 strain (DE3) for protein production. All the manipulations were carried out in an anaerobic chamber (Thermo Forma, Inc., Waltham, MA, USA). Briefly, transformants were grown on agar plates (LB medium containing 50 μg/mL of kanamycin) at 37 ℃. Colonies occurred on agar plates were then picked out and inoculated into liquid LB media (containing 50 μg/mL kanamycin) for cultivation at 37 ℃ for 12 h. Grown cells (2 mL) were inoculated into 200 mL of liquid LB medium (containing 50 μg/mL of kanamycin) for further cultivation at 37 ℃. When their biomass (OD_{600}) reached ~ 0.8, protein expression was induced at 16 ℃ with the supplementation of 1 mM IPTG. After 16 h of incubation, *E. coli* cells were harvested by centrifugation at 5,000 *g* for 10 min at 4 ℃, and then resuspended in buffer (50 mM Tris-HCl, 100 mM NaCl, 10% glycerol, pH 7.9). Cells were lysed using a cell disruptor (French Press, Constant Systems Limited, UK), and the lysate was clarified by centrifugation at 12,000 *g* for 1 h at 4 ℃. The supernatant was loaded onto a Ni^{2+} Sepharose™ 6 fast flow agarose column (GE Healthcare, Waukesha, WI, USA) for purification. The column was then washed with 150 mL protein solution A (20 mM Tris-HCl, pH 7.9, 10% glycerol, 500 mM KCl, 10 mM imidazole) followed by 150 mL protein solution B (20 mM Tris-HCl, pH 7.9, 10% glycerol, 500 mM KCl, 25 mM imidazole) and 300 mL protein solution C (20 mM Tris-HCl, pH 7.9, 10% glycerol, 500 mM KCl, 50 mM imidazole). The elute fractions from solution C (containing target proteins) were applied to an Amicon Ultra 15 Centrifugal Filter (Milipore Billerica MA) for desalting and imidazole removal using a buffer containing 50 mM Tris-HCl (pH 7.9), 100 mM NaCl, 10% (v/v) glycerol, and 3 mM DTT. The purified protein was stored in 50% (w/v) glycerol at −80 ℃.

Identification of degradation products from acarbose

The identities of the degradation products from acarbose were determined as described below by using a LC-MS spectrometer detector (Q Exactive, Thermo Fisher Scientific, USA). Briefly, a mixture that contained 0.00087 μM of purified Apg (acarbose hydrolase), 2 mg/mL acarbose, and 1 mL of buffer (50 mM Tris-

HCl, 100 mM NaCl, 10% glycerol, pH 7.9) was incubated at 37 ℃ for 30 min. The control was the same mixture except that the heat-inactivated Apg protein. The reaction was stopped by heating at 100 ℃ for 5 min.

Next, samples were analyzed by a Q Exactive quadrupole orbitrap high resolution mass spectrometry coupled with a Dionex Ultimate 3000 RSLC (HPG) ultra-performance liquid chromatography (UPLC-Q-Orbitrap-HRMS) system (Thermo Fisher Scientific), with a HESI ionization source. In brief, samples (the injection volume was 2 μL) were firstly separated with an ACQUITY UPLC HSS T3 column (100 mm × 2.1 mm, 1.8-μm particle size; Waters). The mobile phase consisted of solution A (2 mM ammonium formate and 0.1% formic acid in water) and solution B (acetonitrile and methanol, 1:1). The gradient elution was set as follows: 0–0.5 min, 1% B; 0.5–15 min, 1–30% B; 15–20 min, 30%—90% B; 20–25 min, 90% B; 25.1–30 min, 1% B. The flow rate was 0.3 mL/min and column temperature was 45 ℃. All MS experiments were performed in positive and negative ion modes using a heated ESI source. The source and ion transfer parameters applied were as followed: spray voltage 3.5 kV (positive) and 2.8 kV (negative). For the ionization mode, the sheath gas, aux gas, capillary temperature, and heater temperature were maintained at 40, 10 (arbitrary units), 275 ℃ and 350 ℃, respectively. The S-Lens RF level was set at 50. The Orbitrap mass analyzer was operated at a resolving power of 70,000 in full-scan mode (scan range: 200—1200 m/z; automatic gain control (AGC) target: 1e6) and of 175.00 in the Top 3 data-dependent MS2 mode (stepped normalized collision energy: 10, 20, and 30; injection time: 50 ms; isolation window: 4 m/z; AGC target: 1e5) with a dynamic exclusion setting of 5.0 seconds.

Determination of the inhibition of acarbose, acarviosine-glucose, and acarviosine on α-amylase activity

The inhibitory effect of acarbose on α-amylase was determined as previously described[25]. Briefly, a mixture (50 μL) containing 5 μL porcine pancreatic α-amylase (50 U/ml) (10080-25G, Sigma Aldrich, USA), 100 mM acarbose, 100 mM acarviosine-glucose, and 100 mM acarviosine was pre-incubated at 20 ℃ for 10 min, followed by addition of 100 μL of 0.2% soluble starch (dissolved in 100 mM phosphate buffer, pH 6.9) and incubation at 20 ℃ for 30 min. The reaction was terminated by adding 20 μL of 1 M HCl. The residual starch in the reaction mixture was determined as follows: 100 μL of the reaction mixture was mixed with 25 μL of Lugol's iodine solution (G1069, solarbio, China). The absorption of the mixture at 630 nm was measured using a microplate reader (CLS3922-100EA, Corning, USA). The concentration of starch was calculated by comparing the absorption of the samples to the standard curve for soluble starch. Each assay was repeated in triplicate.

Apg enzyme assays and kinetics

All the assays were performed in an anaerobic chamber (Thermo Forma, Inc., Waltham, MA, USA). Briefly, the buffer contained 50 mM Tris-HCl (pH 7.9), 100 mM NaCl, 10% (v/v) glycerol, and 3 mM DTT. The reaction mixture (200 μL) containing 0.00087 μM Apg, 2 mg/mL of substrates (acarbose, maltopentaose, maltotriose, maltotetraose, starch, maltose, or isomaltotriose), and buffer was incubated at 37 ℃ for 10 min. The reaction was terminated by heating at 100 ℃ for 5 min. The reaction mixture was then

centrifuged at 14,000 *g* for 10 min at 4 ℃, and the supernatant was used to determine glucose concentration. Each assay was repeated in triplicate.

The concentration of the purified Apg protein was determined using the Bio-Rad assay reagent (Bio-Rad Laboratories, Hercules, CA, USA) with bovine serum albumin as a standard. One unit of Apg activity (U) was defined as the amount of enzyme that catalyzes the formation of 1.0 μmol of glucose per minute under the given experimental conditions.

To determine the K_m and k_{cat} values of Apg for acarbose under anaerobic conditions, this enzyme was tested at a concentration ([E]) of 0.00087 μM with various concentrations ([S]) of the substrates (acarbose) in the reaction system. The reaction mixture (200 μL) that contained 50 mM Tris-HCl (pH 7.9), 100 mM NaCl, 10% (v/v) glycerol, 3 mM DTT, 0.00087 μM purified Apg, and different concentrations of acarbose (0.09, 0.15, 0.22, 0.31. 0.46, 0.93, 1.55, 2.79, 3.72, 4.65, 5.27, and 6.20 μM) was incubated at 37 ℃ for 5 min. The reaction was terminated by heating at 100 ℃ for 5 min. The reaction mixture was then centrifuged at 14,000 *g* for 10 min at 4 ℃. The supernatant was used to determine acarbose consumption by HPLC. Initial rates of substrate consumption (V) were obtained by linear regression of the data points within the initial reaction time (0–5 min) (the substrate consumption versus time). The observed rate constant (k_{obs}) was calculated according to the equation (k_{obs} = V/[E]), and then fit to the equation, $k_{obs} = k_{cat} * [S]/(K_m + [S])$, in Graphpad Prism, yielding K_m and k_{cat} values.

Phylogenetic analysis of Apg homologs

The protein sequence of Apg was used as the query for a BLASTp search against the non-redundant protein database at NCBI. The resulting Apg homologues with identity no less than 80% were selected with the removal of duplicates and unclassified entries according to their descriptions. For a better visualization, at most five Apg homologues within a genus were adopted. The chosen protein sequences were aligned using the MUSCLE algorithm in MEGA11[26] with the default setting. A maximum likelihood phylogenetic tree was generated from this alignment in MEGA11 with the default setting and tested by bootstrapping 100 times. At last, the taxonomic information was highlighted with different colors manually.

Assessment of the prevalence and abundance of Apg$^+$ bacteria in human gut microbiome

The protein sequence of Apg was used as the query for a BLASTp search against the non-redundant protein database at NCBI to obtain its homologues. Taxa containing Apg homologue genes (identity ≥ 85%, 42 in total) were selected as Apg$^+$. Meanwhile, the taxonomic abundances of healthy human and type 2 diabetes patient intestinal bacterial metagenome samples and their meta-information were downloaded from GMrepo (https://gmrepo.humangut.info/home) with the phenotype ID of D006262 and D003924. We only kept the samples generated by metagenomics but not amplicon, QC passed, and not using antibiotic recently. For the metagenomic samples generated in this study, we annotated and summarized the abundances of all the genes belonging to a specific species. The summarized

abundance of Apg^+ bacteria was calculated as the summation of all Apg^+ taxa abundances in a sample. Samples with a summarized abundance greater than 95% of all the samples were considered as technical outliers and excluded. A sample presenting more than 0.01% of the summarized abundance was defined as Apg^+.

DNA extraction, library construction, and metagenomic sequencing

The E.Z.N.A.® Soil DNA Kit (Omega Bio-Tek, Norcross, GA, U.S.) was adopted to extract genomic DNA from patient stool samples according to the manufacturer's method. The concentration and purity of the extracted DNA were evaluated using a micro fluorometer (TBS-380, TurnerBioSystems, USA) and NanoDrop spectrophotometer (NanoDrop 2000, Thermo Fisher Scientific, Waltham, MA), respectively. The quality of the extracted DNA was examined by visualizing the DNA using agarose gel electrophoresis (1% agarose gel).

Then, the extracted DNA was fragmented to an average size of ~ 400 bp by sonication with a Covaris M220 sonicator (Gene Company Limited, China). The paired-end library was constructed by using the NEXTflexTM Rapid DNA-Seq Library Prep Kit (Bioo Scientific, Austin, TX, USA). Adapters containing the full complement of sequencing primer hybridization sites were ligated to blunt-ends of fragments. Paired-end sequencing was performed on Illumina NovaSeq/Hiseq Xten (Illumina Inc., San Diego, CA, USA) at Majorbio Bio-Pharm Technology Co., Ltd. (Shanghai, China) using NovaSeq Reagent Kits/HiSeq X Reagent Kits according to the manufacturer's instructions (www.illumina.com).

Raw data processing and bioinformatics analysis

The raw reads from metagenome sequencing were cleaned by trimming adaptor sequences and removing low-quality sequences using the fastp[27] (https://github.com/OpenGene/fastp, version 0.20.0) on the Majorbio Cloud Platform (cloud.majorbio.com). The remaining clean reads were mapped to the human hg38 reference genome using BWA[28] (http://bio-bwa.sourceforge.net, version 0.7.9a) to identify and remove the human host originated reads. These high-quality reads were then assembled to contigs using MEGAHIT[29]. Contigs with the length being or over 300 bp were selected as the final assembling result.

Bioinformatics analysis of metagenomic data was performed as previously described[30–32], including the construction of non-redundant gene sets, functional enrichment analysis, and species annotation under different taxa[33]. Briefly, the clean reads after quality control were mapped to representative gene sequences (95% identity) using SOAPaligner. Based on the NCBI NR database, we annotated gene sets for viruses, bacteria, fungi, protozoa, and archaea using Diamond (version 0.8.35). In the generated unified database, each gene is assigned to a highest-scoring taxonomy, which facilitates simultaneous assessment of these microbial species in the gut ecosystem of patients with T2DM. One-way analysis of variance (ANOVA) was used to analyze the diversity parameters (ACE and Simpson) of the gut microbiota of diabetes at different response acarbose-treatment (high-response group and low-response group). T-

test was performed to analyze the bacteria with the highest abundance (phylum and species) in the gut of different response acarbose-treatment.

Molecular modeling of Apg

The enzyme-ligand complex 3D structure was processed using Protein Preparation in Schrödinger/2020-4 (Schrödinger, LLC, New York, NY), including assigning bond orders using CCD database, adding hydrogens, creating zero-order bonds to metals, creating disulfide bonds, optimizing H-bond assignment, and restrained minimization. Then, a docking grid was defined around the centroid of the ligand with a similar size of the ligand using Glide in Schrödinger/2020-4. Meanwhile, 3D structures of the small molecules of interest (i.e., acarbose and its derivatives, and other potential substrates of Apg) were processed by LigPrep in Schrödinger/2020-4, retaining the neutralized form and specified chiralities. Finally, each small molecule was docked into the catalytic site of the enzyme using Glide in Schrödinger/2020-4 and scored by the XP mode with expanded sampling, except that the conformation of acarbose binding to human α-amylase was extracted from PDB 1XCX. The docking scores in the result files were taken as estimations of ΔG (kcal/mol)

Data availability

Data supporting the findings of this study are available within the paper and the Supplementary Information files. *K. grimontii* TD1 genome sequencing raw data is available through NCBI-Genome associated with NCBI-Bioproject accession PRJNA801205. All RNA-seq raw data is available through NCBI-SRA associated with NCBI-Bioproject accession PRJNA801096. Datasets and strains generated and analyzed in the study are available from the corresponding author upon reasonable requests. A reporting summary for this Article is available as a Supplementary Information file.

Code availability

The amino acid sequences of enzymes (containing EC numbers) for SSN analysis were downloaded from KEGG. The generated source code is available at https://github.com/lovingstudy/Apg_gut.

Declarations

Corresponding authors

Correspondence to Yang Gu, Guijun Qin, or Weihong Jiang.

Acknowledgments

We are grateful to Yong Wang, Jianlin Xu, Xiaoyan Xu and Yinig Liu for HPLC and LC-MS/MS analysis. We thank Yu Zhang and Hongwei Zhang for Fast protein liquid chromatography (FPLC) analysis. We also thank Zhiping Zhang for field emission scanning electron microscopy (FESEM) analysis. This work was supported by grants from the National Natural Science Foundation of China (31921006 and 82170839).

Author Contributions

J.T., W.J., G.Q., Y.G., Q.S., and G.Z. conceived and initiated the project; J.T. and Z.D. performed the biochemical experiments; C.L., Y.X., F.X., L.W., Y.M., X.G., and G.Q. recruited volunteers and collected the sample; Y.Y., P.Y., and Q.S. performed the animal experiments; J.X. performed the docking experiments and prepared graphical illustrations; W.J., Y.G., J.T., Z.D., J.X., Y.Y., C.L., and Y.X. wrote the manuscript.

Competing interests

The authors declare no competing interests.

References

1. Tseng, T.-S. *et al.* Sugar intake from sweetened beverages and diabetes: A narrative review. World J Diabetes **12**, 1530–1538, (2021).
2. Weng, J. *et al.* Standards of care for type 2 diabetes in China. Diabetes Metab Res Rev **32**, 442–458, (2016).
3. Jia, W. *et al.* Standards of medical care for type 2 diabetes in China 2019. Diabetes Metab Res Rev **35**, e3158, (2019).
4. Balaich, J. *et al.* The human microbiome encodes resistance to the antidiabetic drug acarbose. Nature **600**, 110–115, (2021).
5. Anne E. Martin. *et al.* Acarbose: An α-glucosidase inhibitor.American Journal of Health-System Pharmacy **53**(**19**), 2277–90, (1996).
6. Chiasson, J.-L. *et al.* Acarbose for prevention of type 2 diabetes mellitus: the STOP-NIDDM randomised trial. The Lancet **359**, 2072–2077, (2002).
7. Clissold, S. P. & Edwards, C. A Preliminary Review of its Pharmacodynamic and Pharmacokinetic Properties, and Therapeutic Potential. Drugs **35**, 214–243, (1988).
8. Martin, A. E. & Montgomery, P. A. Acarbose: An α-glucosidase inhibitor. American Journal of Health-System Pharmacy **53**, 2277–2290, (1996).
9. Gu, Y. *et al.* Analyses of gut microbiota and plasma bile acids enable stratification of patients for antidiabetic treatment. Nat Commun **8**, 1785–1785, (2017).
10. Baxter, N. T., Lesniak, N. A., Sinani, H., Schloss, P. D. & Koropatkin, N. M. The Glucoamylase Inhibitor Acarbose Has a Diet-Dependent and Reversible Effect on the Murine Gut Microbiome. *mSphere* **4**, e00528-00518, (2019).
11. Zhang, L. *et al.* Alpha-Glucosidase Inhibitors Alter Gut Microbiota and Ameliorate Collagen-Induced Arthritis. Front Pharmacol **10**, 1684–1684, (2020).
12. Maini Rekdal, V., Bess, E. N., Bisanz, J. E., Turnbaugh, P. J. & Balskus, E. P. Discovery and inhibition of an interspecies gut bacterial pathway for Levodopa metabolism. Science **364**, eaau6323, (2019).
13. Klünemann, M. *et al.* Bioaccumulation of therapeutic drugs by human gut bacteria. Nature **597**, 533–538, (2021).

14. Scott, T. A. *et al.* Host-Microbe Co-metabolism Dictates Cancer Drug Efficacy in C. elegans. Cell **169**, 442–456.e418, (2017).
15. Javdan, B. *et al.* Personalized Mapping of Drug Metabolism by the Human Gut Microbiome. Cell **181**, 1661–1679.e1622, (2020).
16. Kathrin A. T., *et al.* Genotypes of Klebsiella oxytoca isolates from patients with nosocomial pneumonia are distinct from those of isolates from patients with antibiotic-associated hemorrhagic colitis. Journal of Clinical Microbiology **52**,1607–16, (2014).
17. Breitmeier, D., Günther, S. & Heymann, H. Acarbose and 1-Deoxynojirimycin Inhibit Maltose and Maltooligosaccharide Hydrolysis of Human Small Intestinal Glucoamylase–Maltase in Two Different Substrate-Induced Modes. Archives of Biochemistry and Biophysics **346**, 7–14, (1997).
18. Pastor, A. *et al.* Role of N-terminal region of Escherichia coli maltodextrin glucosidase in folding and function of the protein. Biochimica et Biophysica Acta (BBA) - Proteins and Proteomics **1864**, 1138–1151, (2016).
19. Dai, D. *et al.* GMrepo v2: a curated human gut microbiome database with special focus on disease markers and cross-dataset comparison. Nucleic Acids Res **50**, D777-D784, (2022).
20. Santilli, A. D., Dawson, E. M., Whitehead, K. J. & Whitehead, D. C. Nonmicrobicidal Small Molecule Inhibition of Polysaccharide Metabolism in Human Gut Microbes: A Potential Therapeutic Avenue. ACS Chemical Biology **13**, 1165–1172, (2018).
21. Zhao, B. *et al.* Protective effects of acarbose against insulitis in multiple low-dose streptozotocin-induced diabetic mice. Life Sciences **263**, 118490, (2020).
22. Rajakovich, L. J., Fu, B., Bollenbach, M. & Balskus, E. P. Elucidation of an anaerobic pathway for metabolism of l-carnitine-derived γ-butyrobetaine to trimethylamine in human gut bacteria. Proc Natl Acad Sci U S A **118**, e2101498118, (2021).
23. Livak, K. J. & Schmittgen, T. D. Analysis of Relative Gene Expression Data Using Real-Time Quantitative PCR and the 2 − ΔΔCT Method. Methods **25**, 402–408, (2001).
24. Zhai K, *et al.* NLRs guard metabolism to coordinate pattern- and effector-triggered immunity. Nature**601**(**7892**), 245–251(2022).
25. Liu, H.-L. *et al.* Acylated Aminooligosaccharides with Inhibitory Effects against α-Amylase from Streptomyces sp. HO1518. Mar Drugs **16**, 403, (2018).
26. Tamura, K., Stecher, G. & Kumar, S. MEGA11: Molecular Evolutionary Genetics Analysis Version 11. Mol Biol Evol **38**, 3022–3027, (2021).
27. Chen, S., Zhou, Y., Chen, Y. & Gu, J. fastp: an ultra-fast all-in-one FASTQ preprocessor. Bioinformatics **34**, i884-i890, (2018).
28. Li, H. & Durbin, R. Fast and accurate short read alignment with Burrows-Wheeler transform. Bioinformatics **25**, 1754–1760, (2009).
29. Li, D., Liu, C.-M., Luo, R., Sadakane, K. & Lam, T.-W. MEGAHIT: an ultra-fast single-node solution for large and complex metagenomics assembly via succinct de Bruijn graph. Bioinformatics **31**, 1674–

1676, (2015).
30. Noguchi H, Park J, Takagi T. MetaGene: prokaryotic gene finding from environmental genome shotgun sequences. Nucleic Acids Research **34(19)**, 5623–5630, (2006).
31. Fu L, Niu B, Zhu Z, Wu S, Li W. CD-HIT: accelerated for clustering the next-generation sequencing data. Bioinformatics **28(23)**, 3150–3152, (2012).
32. Li R, Li Y, Kristiansen K, Wang J. SOAP: short oligonucleotide alignment program. Bioinformatics, **24(5)**, 713–714, (2008).
33. Buchfink B, Xie C, Huson DH. Fast and sensitive protein alignment using DIAMOND. Nature Methods **12(1)**, 59–60, (2015).

Figures

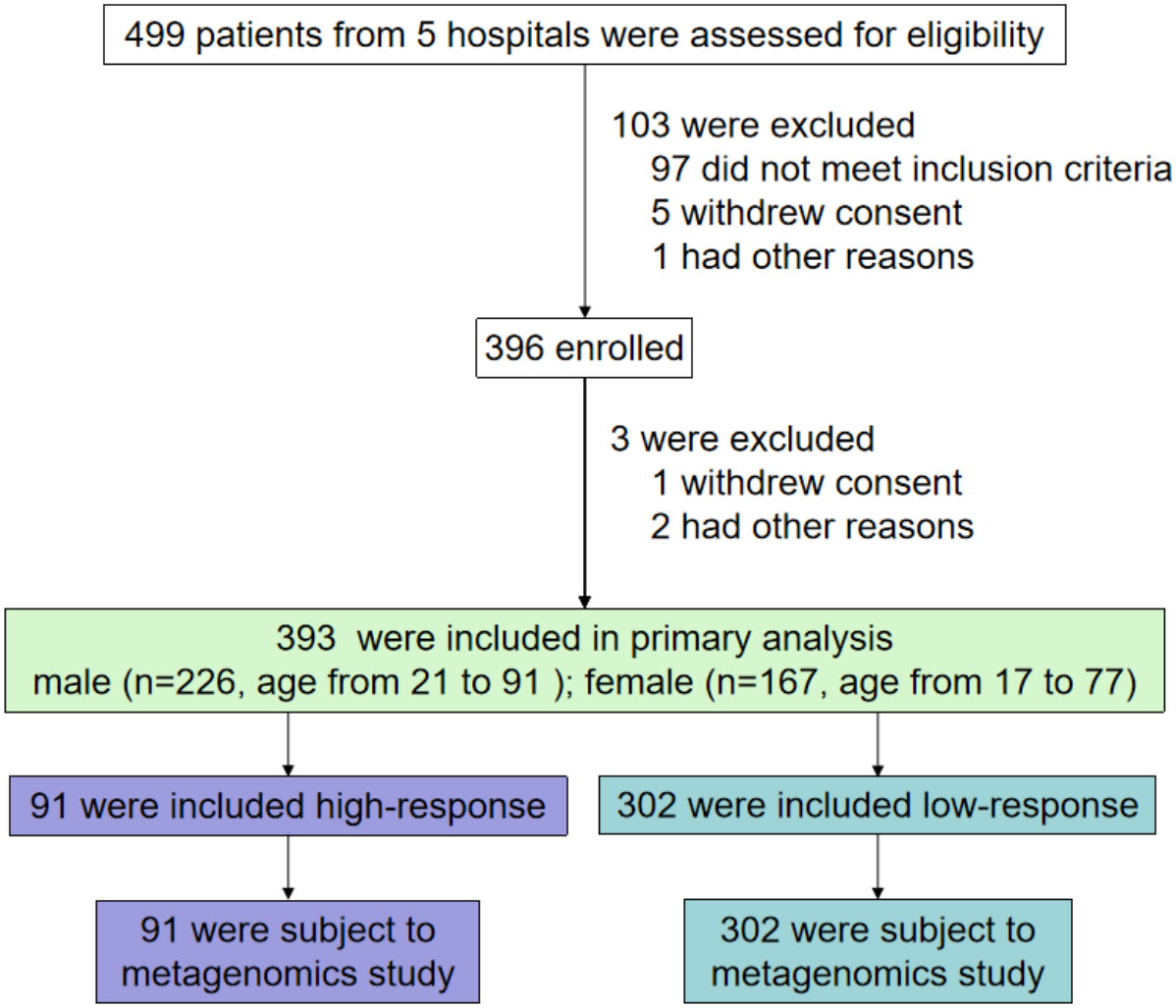

Figure 1

Flow diagram of patient enrolment. In this human observational study, a total of 499 T2DM patients were screened, in which 396 patients were enrolled based on inclusion and exclusion criteria. Inclusion criteria: type 2 diabetes mellitus; individuals treated with acarbose; provision of written informed consent. Exclusion criteria: severe gastrointestinal disease; history of intestinal surgery or abdominal surgery; individuals treated within the last three months with immunosuppressive agents, steroids, antidiarrhea agents, antibiotics, and/or other gastrointestinal motility agents; severe liver dysfunction (serum alanine aminotransferase concentration more than 2.5 times above upper limit of normal range); abnormal renal function (eGFR < 60 ml/min/1.73m2); history or presence of cancer; other severe conditions which would put the patients in high risk during the study. Finally, 393 of the enrolled patients were included in the analyses, while one withdrew consent and two had other reasons. According to the response to acarbose, these 393 patients were divided into high and low-response groups for the collection of fecal and plasma samples.

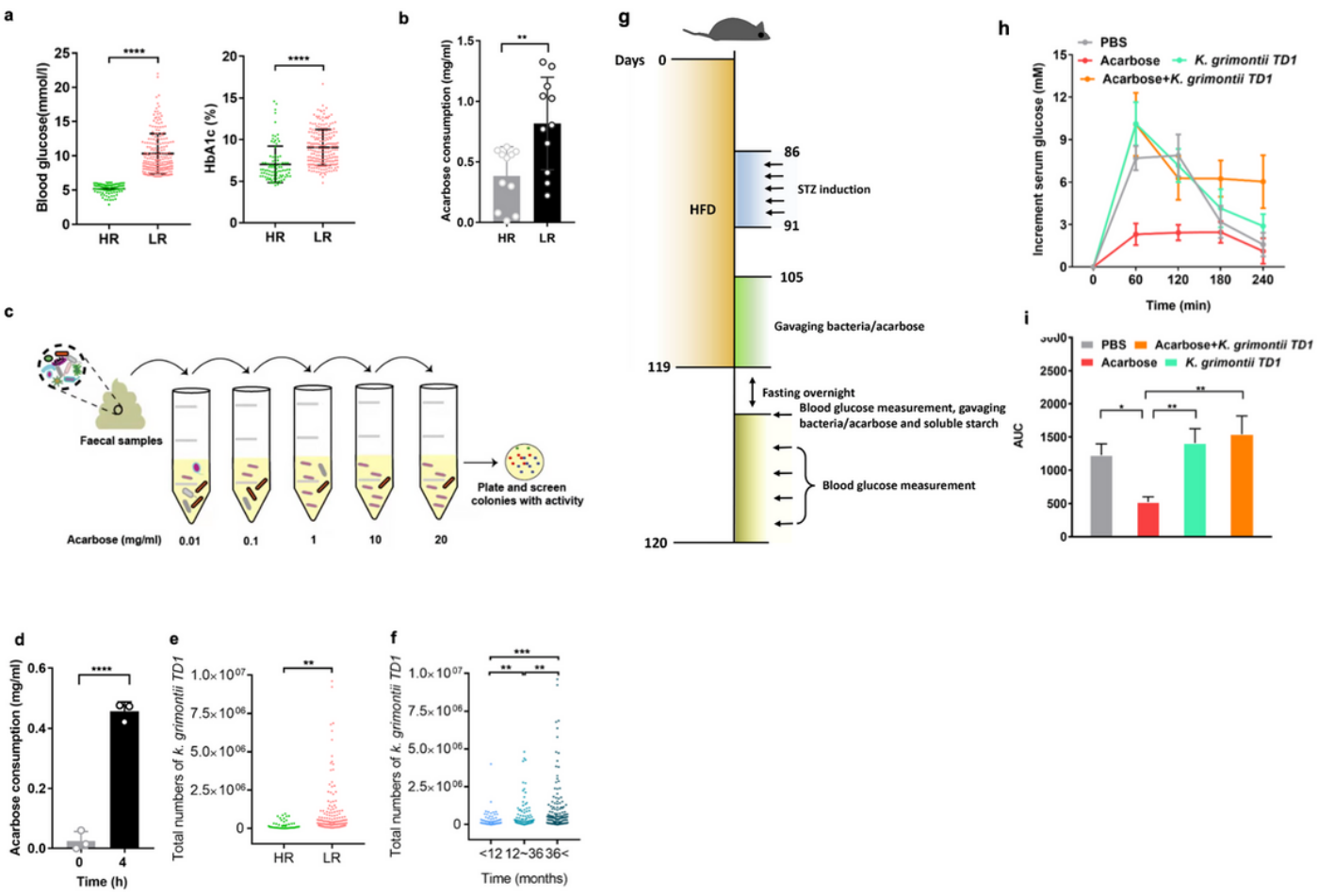

Figure 2

Discovery of an acarbose-degrading *K. grimontii* strain from microbiome of patients with type-2 diabetes. **a**, The blood glucose and glycated haemoglobin (HbA1c) levels of high and low drug response patients with T2DM. The high and low drug response groups were distinguished based on their fasting blood glucose. High response, fasting blood glucose ≤ 6.1; low response, fasting blood glucose > 6.1. HR, high response; LR, low response. **b**, Comparison of acarbose consumption by the microbiome from high and

low drug response patients with type-2 diabetes. **c**, Schematic presentation of enrichment cultivation and isolation of acarbose-consuming strains from human fecal samples. **d**, Evaluation of acarbose consumption by the isolated *K. grimontii* strain. Data are presented as mean ± standard deviation (SD) ($n = 3$). Error bars show SDs. Statistical analysis was performed by a two-tailed Student's *t*-test. ***$p < 0.001$. **e**, The abundance of *K. grimontii* TD1 in gut microbiome from high-drug-responsive and low-drug-responsive patients with type-2 diabetes. **f**, The abundance changes of *K. grimontii* TD1 in patients with different durations in acarbose administration. **g**, Schematic illustration for constructing an HFD/STZ-induced T2DM mouse model and the oral supplementation of acarbose and *K. grimontii*TD1. C57BL/6J mice were fed a high-fat diet for 12 weeks followed by a STZ injection for five consecutive days to induce hyperglycemia. After two weeks, mice with T2DM were screened as having FBG values > 14 mM and then divided into four groups that were administered PBS, acarbose, *K. grimontii* TD1, and *K. grimontii* TD1 + acarbose by gavage. Two weeks later, the mice in the four groups were fasted overnight and administered as abovementioned by gavage the next morning. Simultaneously, all the mice were administered a starch solution (1 g/kg) by gavage. The tail vein blood glucose of each animal was determined using the blood glucose Accu-Chek Performa meter (Roche Diagnostics) at 0, 60, 120, 180, and 240-min post-gavage. The cumulative glucose levels at different time points were calculated and used to evaluate the anti-diabetic effect of acarbose. **h**, **i**, Incremental serum glucose levels (**h**) and areas under the glucose response curve (**i**). Statistical significance of data was determined using one-way analysis of variance (ANOVA) (*$p < 0.05$; **$p < 0.01$; ***$p < 0.001$).

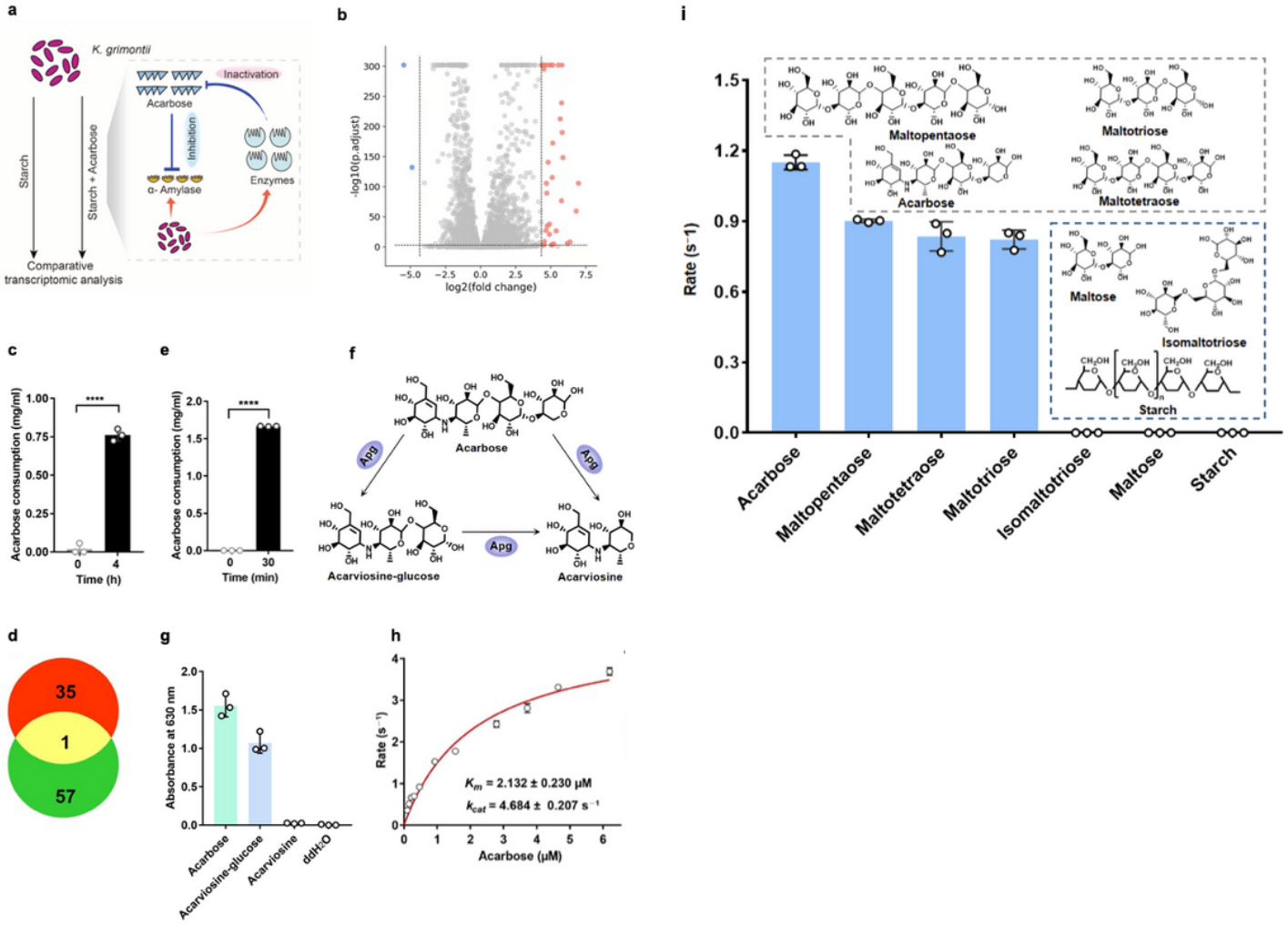

Figure 3

Discovery of an acarbose-preferred glucosidase (Apg) enzyme in *K. grimontii* TD1. a, Design of an acarbose-induced system for identifying potential genes encoding acarbose-degrading enzymes in *K. grimontii* TD1. The presence of acarbose in the medium was expected to cause upregulation of target genes. **b**, Volcano map of differentially expressed genes in *K. grimontii* TD1 in the presence of acarbose (2.0 g/L). Each dot represents one gene. The red and blue dots indicate the genes exhibiting significantly changed expression levels (≥ 20-fold upregulation and downregulation respectively). The other genes are represented by grey dots. **c**, Acarbose degradation by cell lysates of *K. grimontii* TD1 under anaerobic conditions. Data are presented as mean ± SD (n = 3). Error bars show SDs. Statistical analysis was performed using a two-tailed Student's t-test. ****$p < 0.0001$. **d**, Number of the proteins uncovered by the comparative transcriptomic analysis (≥ 20-fold upregulation in gene expression in the presence of acarbose) and FPLC to be potentially associated with acarbose degradation in *K. grimontii* TD1. **e**, *In vitro* validation of the acarbose-degrading activity of the purified Apg under anaerobic conditions. Data are represented as mean ± SD (n = 3). Error bars show SDs. Statistical analysis was performed by a two-tailed Student's t-test. ****, $p < 0.0001$. **f**, Possible acarbose-degrading pathways in *K. grimontii* TD1 mediated by Apg. **g**, Inhibition of acarbose and acarbose-degraded products on α-amylase. The residual starch in the reaction mixture was determined by the absorption at 630 nm. The sample that used ddH2O

(double distilled water) to replace the acarbose-degraded products was set as the negative control. **h**, *In vitro* steady-state kinetic analysis of Apg using acarbose as the substrate. Each data point represents mean ± SD (*n* = 3). Error bars show SDs. **i**, A screening of the substrate spectrum of Apg. Initial turnover rates of the purified Apg towards different substrates (100 μM) were measured. Data are represented as mean ± SD (*n* = 3). Error bars show SDs.

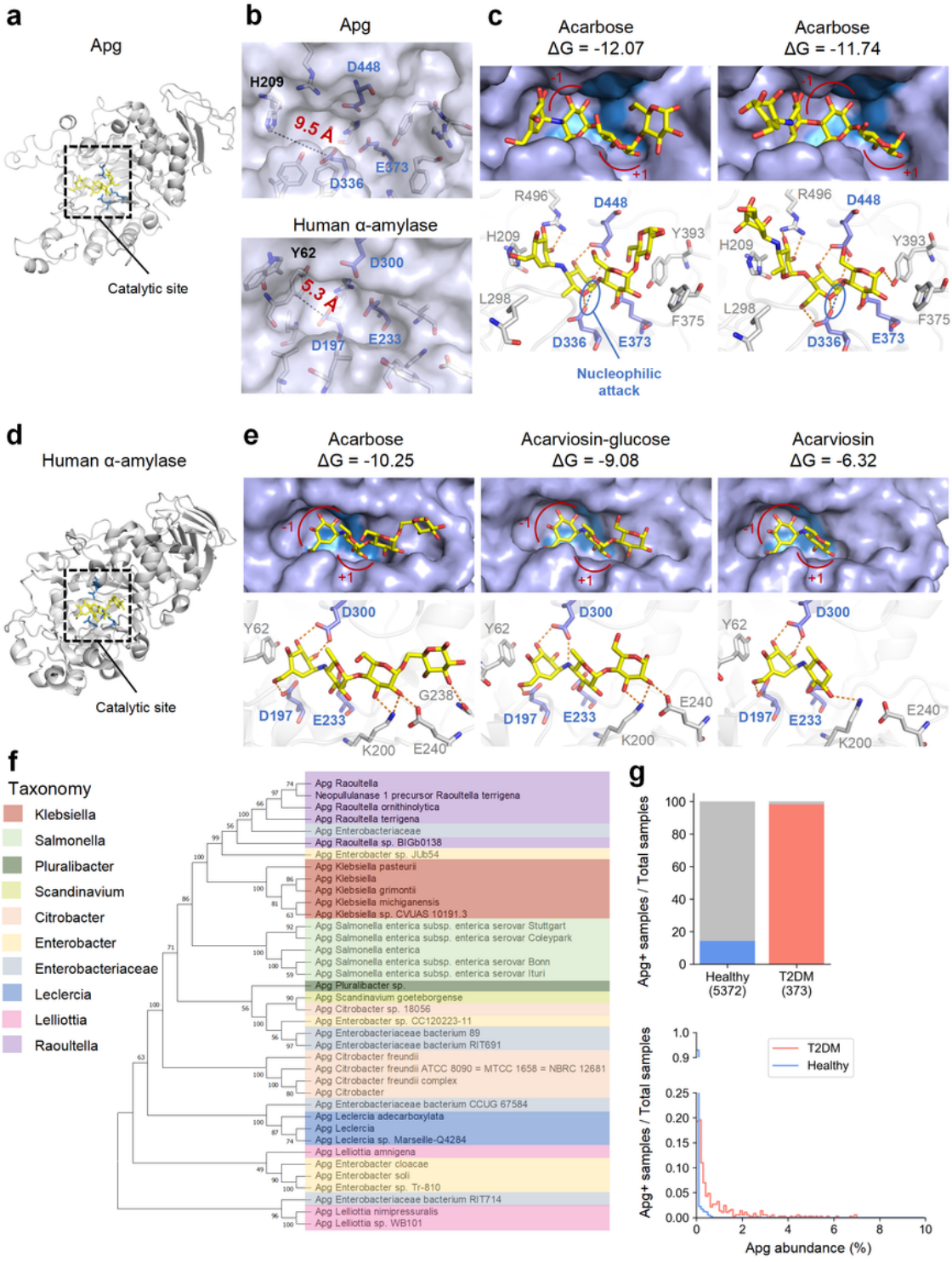

Figure 4

Molecular modeling of the interaction between acarbose and Apg/human α-amylase as well as abundance analysis of *apg*homologs. a, Animated representation of Apg with its catalytic site highlighted. Catalytic residues are shown as blue sticks. The ligand is shown as yellow sticks. **b**, Catalytic pockets of Apg (top) and human α-amylase (bottom). The distances between the nucleophile residue and the margin of the pocket are denoted in red. **c**, Surface views (the top row) and residue views (the bottom row) of the two patterns of acarbose binding with Apg at the catalytic site. The values of ΔG (in kcal/mol, estimated by Glide) are displayed under the ligand name. The surface of the binding pocket is colored grey, and the catalytic spot is highlighted with blue. −1 and +1 sugar subsites are labeled. In the residue view panels, catalytic residues are shown in blue sticks. Other residues interacting with the ligands are shown as grey sticks. Names are labeled beside the residues. Orange dashed lines indicate hydrogen bonds. The nucleophilic attack interactions are depicted as blue dashed lines. **d**, Animated representation of human α-amylase. **e**, Surface views and residue views of acarbose, acarviosine-glucose, and acarviosine binding with human α-amylase at the catalytic site. Other annotations are the same as for **c**. **f**, A maximum likelihood phylogenetic tree of Apg homologues across different species and genera (partial screenshot of Supplementary Figure 9). Numbers on the branches indicate bootstrap supports (bootstrap values > 50%). **g**, Prevalence and abundance of *apg* and Apg+bacteria in the intestinal microbiota of healthy human (blue) and patients with T2DM (pink). Embraced numbers indicate the sample size of the categories.

Supplementary Files

This is a list of supplementary files associated with this preprint. Click to download.

- SupplementaryFiguresandTables.docx